CFD Analysis of a Supersonic Air Ejector. Part I: Experimental Validation of Single-Phase and Two-Phase Operation

Amel Hemidi, François Henry, Sébastien Leclaire, Jean-Marie Seynhaeve, Yann Bartosiewicz

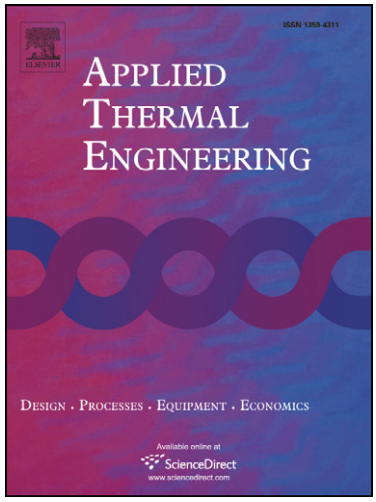

CFD Analysis of a Supersonic Air Ejector. Part I: Experimental Validation of Single-Phase and Two-Phase Operation

Amel Hemidi, François Henry, Sébastien Leclaire, Jean-Marie Seynhaeve, Yann Bartosiewicz

PII: S1359-4311(08)00303-7
DOI: 10.1016/j.applthermaleng.2008.07.003
Reference: ATE 2566

To appear in: *Applied Thermal Engineering*

Received Date: 6 August 2007
Revised Date: 22 May 2008
Accepted Date: 4 July 2008

Please cite this article as: A. Hemidi, F. Henry, S. Leclaire, J-M. Seynhaeve, Y. Bartosiewicz, CFD Analysis of a Supersonic Air Ejector. Part I: Experimental Validation of Single-Phase and Two-Phase Operation, *Applied Thermal Engineering* (2008), doi: 10.1016/j.applthermaleng.2008.07.003

CFD Analysis of a Supersonic Air Ejector. Part I: Experimental Validation of Single-Phase and Two-Phase Operation

Amel Hemidi, François Henry, Sébastien Leclaire,

Jean-Marie Seynhaeve and Yann Bartosiewicz *

Université catholique de Louvain UCL, Faculty of Applied Sciences, Mechanical Engineering Department, TERM Division, Place du Levant 2, B-1348, Louvain-la-Neuve, Belgium. Tel: +32 10 47 22 06, Fax: +32 10 45 26 92

Abstract

This paper deals with comparisons between CFD and experiments for a supersonic ejector. Good results are presented in terms of entrainment rate compared to home-made experimental data for an air ejector. Over the whole range of operating conditions, the overall deviation is below 10% for the $k-\epsilon$ model, while the results for the $k-\omega-sst$ model are in a less agreement. Furthermore, it is demonstrated that the validation of a global performance parameter, such as the entrainment rate, is not sufficient for a correct assessment even though a wide range of operation is tried out. Indeed, for exactly the same prediction both model may give very different local flow features. Finally, a first attempt to tackle two-phase aspects was also performed experimentally and by simulations.

Key words:

Supersonic Ejector, Air-Conditioning, CFD-Experiment Integration, Turbulence

1 Introduction

Supersonic ejectors are simple mechanical devices (Fig. 1(a)), which can be used to pump and compress a given flow without any moving parts. As the primary (1) (Fig. 1(a)) supersonic jet is discharged, by an entrainment-induced effect the secondary stream (2) (Fig. 1(a)) is drawn into the ejector and eventually compressed to the back pressure (b) (Fig. 1(a)). For a detailed flow physics analysis inside ejectors, readers should refer to [1–3]. If the secondary flow reaches sonic conditions the ejector operation is said "on-design", the entrainment rate defined as $\omega = \dot{m}_2/\dot{m}_1$ being maximum. On the contrary, if the secondary flow remains subsonic, the operation is not stable, the entrainment rate strongly decreases and it is said "off-design". The point splitting these two operation zones is then called the critical point. One of the most promising application is the steam jet refrigeration as an environment-friendly technology in a response to the problem of global warming (GHG emissions) or ozone depletion.

In this paper, as presented figure 1(b), the targeted application is the use of supersonic ejectors in air conditioning [4,5] and refrigeration [6,7] areas to realize thermal compression activated by low-grade heat release or a renewable source such as solar energy. In this case the goal is to drawn a maximum secondary flow rate to compress from the evaporator pressure to the condenser pressure.

* Corresponding author
Email address: yann.bartosiewicz@uclouvain.be (Yann Bartosiewicz).

A good overview of the different applications in this field may be found in the review articles of Sun and Eames [8], Chunnanond and Aphornratana [7], and more recently Riffat et al. [9]. However, the development of such systems at industrial scales is limited due their efficiency and stability at off-design conditions raising the problem of their operation and control. Therefore, CFD can be seen as an attractive tool to understand and predict ejector operations and could be then used to perform better design of the ejector itself, if sufficiently validated to be considered as a reliable tool. But a lot of questions still remain and a lot of shortcomings should be avoided. Indeed, most of the studies [10–12] have not performed any sensitivity analysis concerning the turbulence modeling and usually assume that the standard $k-\epsilon$ model is able to give good results although some authors [2, 3, 13, 14] already highlighted the large sensitivity of the chosen turbulence approach depending on the ejector operations. In addition, the authors [2, 13] raised the problem of a rigourous CFD-experiment integration in so far as numerical computations often do not match experiment conditions in terms of boundary conditions (difference between the location and/or the type of measurements compared to CFD) or geometric design (axisymmetric solver-3D ejector configuration). These mismatches often involve some unjustified assumptions or model tunings such as geometry adaptation or boundary conditions adjustments. Moreover previous studies usually focussed on the prediction of the maximum or on-design entrainment rate [10], which is not very challenging in most of the operating conditions, or revealed large discrepancies beyond the critical point [3, 11, 15].

One of last comparative studies [11] showed that CFD predictions could satisfactorily predict the on-design operation and the critical point, but failed in the prediction of the off-design mode since discrepancies of about 40%-50%

could be reached. However, those single-phase results under the perfect gas assumption were compared to a steam flow where two-phase aspects may occur. Very recently, with the same experimental stand, Pianthong et al. [15] showed some validation results where CFD underestimated experimental values up to 16% for the on-design entrainment rate and 13% for the critical point. These differences then involved much more errors for the off-design operation (50%-100%). However, their results [15] clearly show that those discrepancies between CFD and experiment are strongly related with the operating conditions. In addition, Pianthong et al. [15] claimed that 3D and axisymmetric models provided same results. However, they justified this statement for one condition at on-design and for a wall pressure profile, which are probably not relevant to assess this assumption. Indeed, when the secondary flow is not choked, if the same total pressure is prescribed at the secondary inlet, the mass flow rate could be depend on the flow area, which is obviously different in 3D and axisymmetric; for on-design condition the mass flow rate is limited by the critical cross section. Furthermore, it is known that an equivalent axisymmetric area does not provide good results [2, 13] if the real geometry configuration is 3D. Two other big issues yet scarcely addressed are the real gas properties [3, 10] and the non-equilibrium two-phase nature of the flow due to nucleation, condensation, and meta-stable states. To our knowledge the latter point has never been raised and study in literature concerning vapor ejectors operating with refrigerants. Nevertheless, prior to tackle those very complex phenomena, it is very useful to know the limit of numerical simulations in the prediction of the single phase operation over a wide range of operating conditions, and to address some issues such as the sensitivity to the turbulence model over several conditions, the link between the local flow physics and global ejector performances predicted by different models. These aspects

are assessed in this paper with the help of new experimental results. For this purpose a simple test bench working with air has been built to match as far as possible CFD conditions. Also a first attempt to tackle two-phase aspects is conducted numerically and experimentally as Al-Ansary et al. [14, 16] who introduced fine droplets into the primary stream.

2 Modeling Approach

2.1 Governing equations

The choice of air as the working fluid is very useful because it avoids biased results due to a two-phase aspect. In addition, future works will consist of flow visualizations which often require an open access. The flow in the air-ejector is governed by the ideal gas compressible steady-state axisymmetric form of the fluid flow conservation equations. For variable density flows, the Favre averaged Navier-Stokes (FANS) equations are more suitable and will be used in this work. The total energy equation including viscous dissipation is also included and coupled to the set with the perfect gas law. The thermodynamics and transport properties for air are held constant; their influence was not found to be significant during previous tests. In this paper, inert water droplets are injected into the primary flow, as proposed and performed experimentally by Al- Ansary and Jeter [16]. These water droplets are considered spherical and are modelled as a discrete second phase in a Lagrangian frame. In order to take into account the coupling between the continuous and the dispersed phase, a source term is added to the momentum (F_p). Thus for single phase computations, $F_p = 0$.

The trajectories are predicted by integrating the force balance on the particles:

$$\frac{du_p}{dt} = F_D\left(u - u_p\right) \tag{1}$$

where F_D stands for the drag force coefficient per unit particle mass and it is written:

$$F_D = \frac{18\mu}{\rho_p {d_p}^2}\frac{C_D R_e}{24} \tag{2}$$

For the continuous phase the drag source term then becomes in its discretized manner:

$$F_p = F_D\left(u_p - u\right)\dot{m}_p \Delta t \tag{3}$$

The coefficient C_D is calculated according the law of Morsi and Alexander [17]. This set of equations is solved by a control volume approach in the CFD commercial package FLUENT 6.2. Although the steady state is desired, the unsteady term is conserved since from a numerical point of view, governing equations are solved with a time marching technique. This allows to keep equations parabolic-hyperbolic for every Mach number. The system is also time-preconditioned in order to overcome the problem of numerical stiffness at low-mach numbers. The convection term is discretized with a flux splitting method in order to capture shock accurately (second order upwind), while the diffusive term uses a central difference discretization. The coupled system is then solved by a block Gauss-Seidel method with an algebraic multigrid acceleration algorithm. Concerning turbulence modeling, Bartosiewicz et al. [2, 3]

showed from preliminary tests that local behavior in terms of local flow structures is strongly dependent on the turbulence model. However it was difficult to conclude because of possible mismatches between numerical and experimental boundary conditions. For conciseness reasons, the reader is referred to references [2, 3] for more details about the features and performances of these turbulence models or other algorithm features.

2.2 Numerical accuracy and convergence

The criterion for assessing convergence was based on the root mean square of the equation residues expressed by:

$$R(\zeta) = \left[\sum_{i=1}^{N} \left(\frac{\partial \zeta}{\partial t}\right)_i^2\right]^{1/2} \tag{4}$$

where N is the number of grid points and ζ is the considered variable (mass, energy, momentum, etc.). Generally, computation are stopped when residues fall below $1 * 10^{-6}$ and remain stable. In addition, at convergence the mass imbalance is checked and should be:

$$\left|\frac{\sum \dot{m}_{in} - \sum \dot{m}_{out}}{\sum \dot{m}_{in}}\right| \tag{5}$$

The time step is set up by a Courant-Friedrichs-Lewy (CFL) conditions. At the beginning of calculations, it is set to 0.5 because the solution is highly non-linear, and it is increased up to 5 at the end due the implicit time discretization. Moreover, before to proceed deep analysis, a grid convergence study was performed to ensure overall mesh independent results. For instance

the calculated deviations for the primary and secondary mass flow rate were respectively 0.44% and 1.16% for the two different meshes (25820 cells and 88566 cells). In addition figure 3 demonstrates that the results are also locally converged with the coarser mesh.

Finally, mesh 1 (25820 cells) (Fig. 2) was considered sufficient to give satisfactory results in term of entrainment ratio. This mesh is refined from the primary nozzle lips along the shear layer and also close to walls. In most of the cases, the overall value for the wall coordinate is $y^+ \approx 1$, so a one equation low Reynolds model [18] is used (bi-layer model), otherwise a classical wall-function approach is use in areas with a higher y^+.

3 Experimental apparatus

3.1 Description of the experimental set-up

A sketch of the experimental apparatus is given figure 4(a). The experimental apparatus is equipped with the following elements:

- An upstream vessel of 5 m^3 filled with compressed air at about 7 bar.
- A pressure reducer.
- The primary pipe equipped with a flow measuring device.
- The ejector to be tested (Fig. 4(b)).
- The secondary pipe also equipped with a flow measuring device and connected to the atmosphere.
- The exhaust pipe equipped with manual adjustable valve.

The ejector geometry 4b is axisymmetric, the flow at the annular secondary inlet comes from a mixing chamber where the pressure relative to the atmosphere is measured in order to match CFD boundary conditions (axisymmetric solver). The tests of the ejector were conducted at constant driving pressure in the primary pipe which can be finely controlled by the pressure reducer. Four different primary pressures P_1 were tested : 3 bar, 4 bar, 5 bar and 6 bar. For each of these pressures, the back pressure at the exhaust pipe was controlled by the manual valve. The choice of the back pressure was firstly dictated by the total back pressure obtained in the different simulations, the experimental static pressure being roughly equal to its total value at this location: this can be easily checked analytically.

Some tests have been performed with water droplets injection into the primary air stream. These droplets were produced by an ultrasonic atomizer (UCL patent 09900790) spray, which is able to create a quasi monodispersed granulometric curve of droplets. The chosen atomizer provided droplets of 50 μm in diameter.

3.2 Description of the instrumentation

The pressures P_1 and P_b are measured by effective pressure transducers which have been previously calibrated with a manometric balance. The differential pressure transducers used in the flow measuring devices have been calibrated with a Betz manometer. These calibrations have been carried out just before the experimental campaign. The temperatures are measured by PT100 sensors of type A which ensure an uncertainty less than 0.1 $^{\circ}C$. The mass flow rates are determined from an orifice plate device equipped with 1D and 1/2

D pressure taps according to the ISO 5167 standard. The uncertainties on all the quantities (pressures, temperatures, mass flow rates, etc.) have been determined according to the Guide of Uncertainties on Measurements (GUM). These uncertainties have been reported in figure 5 for the entrainment rate. In this figure, some typical ejector characteristics can be observed, i.e. the entrainment rate ω as a function of the compression rate. These curves are characterized by a constant mass flow rate corresponding to a choked secondary flow or on-design conditions, followed by a significant decrease of the secondary mass flow rate or off-design conditions.

4 Results and discussions

4.1 CFD validation: single-phase flow

For this validation part, the main dimensions of the ejector are depicted figure 6. The total length of the ejector is $22.5mm$ for 25820 cells. Originally, this geometry was designed for a real refrigeration cycle using butane as the working fluid and follows the ESDU [19] and ASHRAE [20] prescriptions. In this paper, this ejector is tested with air in order to assess CFD models in terms of operation features for a broad range of conditions. Therefore, the geometry characteristics such as the distance between the primary nozzle and the inlet of the mixing chamber is kept constant to $\Delta L = 3D^*$, $d^* = 3.3mm$, $d = 4.5mm$, $D^* = 7.6mm$.

As our interest is focus on refrigeration applications, it is relevant to sweep the different ejector operation modes by changing the back pressure P_b for constant primary and secondary pressures P_1 and P_2. Indeed, for this case,

the back pressure would be that of the condenser which is strongly dependent of the ambient conditions. The secondary pressure is roughly constant during a test series and equal to the atmospheric pressure corrected by the pressure difference measured in the mixing chamber; it is measured for each tested conditions and incorporated in the CFD model. In addition, both the primary and secondary pressures measured are static pressures; their values are incorporated in the CFD model as total pressures in so far as the respective velocities have been calculated to few meters per second providing static and total pressures equal at these locations. For the back pressure the strategy is different: In the experiment, an additional diffuser enlarging the section has been set at the ejector outlet in order to measure an average static pressure equal to the total pressure (very low velocity). In the model, an outlet static pressure is prescribed, the simulation results then provided an average outlet total pressure. This pressure was set in the experiment by using the very accurate control valve at back (Fig. 4(a)). This method is more relevant since in a real system the pressure imposed by the condenser is equivalent to a total pressure because the dynamics pressure is negligible contrary to the ejector outlet where the velocity may be high. Consistently with measurements, the four cases $P_1^0 = 3bar$, $P_1^0 = 4bar$, $P_1^0 = 5bar$ and $P_1^0 = 6bar$ have been carried out. For those cases, the turbulence intensities and the viscosity ratios at inlets were prescribed to $I_{\%} = 0.05$ and $\mu_t = 2 * \mu_l$ according to a fully turbulent pipe flow. All the walls are assumed adiabatic. Figures 7 and 8 illustrate the results in comparison with experimental data. First of all, the general shape of the ejector characteristics curves is well reproduced by CFD, as noted by some authors [11, 14]: as the back pressure is decreased down to a critical pressure, the entrainment ratio $\omega = \dot{m}_2/\dot{m}_1$ increases up to reach a plateau where the secondary mass flow rate and thus ω remain constant.

At this pressure and below, the ejector is said choked and works at on-design conditions. For a higher P_b it operates at off-design conditions. The overall results show that CFD tends to slightly overestimate the maximum entrainment rate, which is in contradiction to Sriveerakul and al. [11] and Pianthong et al. [15] observations.

Contrary to previous last studies [10–12, 15] in literature, the issue of the turbulence modeling is raised and quantitative comparisons can be drawn over the on-design and off-design conditions for different driving pressures. The classical $k-\epsilon$ model is compared to the $k-\omega-sst$ which is supposed to contain a more physical description of the turbulence. Both models include a compressibility term which is slightly different from one to the other. More details about difference between both formulation can be found in [2, 13].

Figures 7 and 8 demonstrate that the different behaviors between $k-\epsilon$ and $k-\omega-sst$ turbulence models depend on the primary pressure. As the primary pressure is decreased, the discrepancies between both models become larger. The differences first appear for the off-design conditions (Fig. 8(a-b)) and become more important over all conditions as the primary pressure is decreased (Fig. 7(b-a)). This feature has never been raised before and it is very relevant since the $k-\omega-sst$ is likely to provide more consistent local flow physics. However, it appears this model significantly over-predicts the entrainment rate for low motive pressures. Nevertheless, for higher primary pressures, the $k-\omega-sst$ model gives similar results for the on-design conditions, and it is slightly better at large off-design conditions where the entrainment becomes very low (Fig. 7(b) and Fig. 8(d)). In terms of experiments and CFD comparisons, the agreement is very good especially for the $k-\epsilon$ for both the on-design conditions, the critical point and in a less sense for the off-design

conditions.

The error distributions compared to experimental points for each model and for $P_1^0 = 4bar$, $P_1^0 = 5bar$ and $P_1^0 = 6bar$ (on-design, off-design) are gathered figures 9(a) and 9(b). The point concerning $P_1^0 = 3bar$ are not represented because for this primary pressure it was not possible to reach a significant range of on-design conditions. Furthermore, for these conditions, the discrepancies for both model are obvious, the $k - \epsilon$ providing very good agreement compared to the $k - \omega - sst$. Figure 9 clearly demonstrates that overall results are better for the $k - \epsilon$. Contrary to recent studies [11,15] the relative difference is mostly below 10% over the whole range of operations (on-design, off-design) and over all driving pressures. For the $k - \omega - sst$, the overall discrepancies are larger but mostly about 10%-20%. However, at low entrainment rate, near flow reversal at the secondary outlet, the $k - \omega - sst$ should be considered and a more specific study should be conducted at this operation when the ejector does not properly work. The current test stand does not allow to measure negative secondary flow rates, and measurements become extremely sensitive to the back pressure at higher compression rate. Finally, figure 10 points out an interesting issue concerning the link between the local flow features and the global ejector performance predicted by those two turbulence models. Indeed, for $P_1^0 = 5bar$ and $P_b/P_2^0 = 1.3$ figure 8(b) shows that both models predict exactly the same entrainment rate, which is the key parameter of the ejector for refrigeration applications. However, figure 10 demonstrates that the prediction of a local flow feature such as the Mach number can be very different. For instance, the $k - \omega - sst$ model provides a strong shock cell, probably a Mach disk, compared to the $k - \epsilon$ results. Furthermore the values of the Mach number in the secondary nozzle and mixing section are very different,

the $k-\omega-sst$ model being less dissipative. This proves that even though the flow structures are very different along the ejector, the predicted entrainment rate can be in agreement. The explanation of such a behavior deserves a further study and will be the scope of a next publication. This results shows that turbulence modeling cannot be assessed only upon global results and it raises the problem of local flow structures validation such as visualizations.

4.2 Two-phase flow aspects

As mentioned in introduction, the only study about the effect of two-phase flow on vapor ejector operation is that of Al-Ansary et al. [16]. In this experiment, fine water droplets ($17\mu m$ according to the manufacturer) are injected at the primary inlet owing to a two-phase atomizer. In their paper, authors [16] reported a significant increase of the entrainment ratio when water droplets are injected, and this effect was only observed at off-design conditions and for low primary pressure (below 2.5 bar). Their increase reached 98% in the best case. However, some inherent limitations were not discussed such as wall effects which can prevent all the water injected to cross the ejector because of water accumulation, possible vaporization-condensation effect in the core flow. In addition, the definition of the two-phase entrainment ratio did not take into account the water mass flow rate and the additional compressed air supplied to the atomizer, which is able to moderate the improvement. In this study, water droplets are injected with an ultra-sonic atomizer which does not need any additional air to atomize water; this is achieved through a vibrating device at a specific resonance frequency. In addition, a purge system was set up to recover and measure the amount of water that did not cross the

ejector because of upstream accumulations. This device allowed to measure the average water mass flow rate during an experiment : for instance, it was found that 22.3% of water was lost at a total water flow rate of $0.5l.h^{-1}$. For those tests, the two previous ejector characteristics, for $P_1^0 = 4bar$ and $P_1^0 = 5bar$, have been remeasured and compared according to the type of flow: results are presented figure 11. For both conditions, the average water mass fraction injected at the primary inlet is roughly the same and about 1%, which is much less than that used by Al-Ansary et al. [16] (about 10% maximum). Figure 11 clearly illustrates that the presence of water droplets has no significant effect at on-design operation. But this effect becomes significant at critical point and beyond at off-design operation (10%-40%). It can be observed that the critical point is slightly moved toward higher back pressures, providing a potential extent of the on-design operation. At off-design operation, the maximum difference at low entrainment rate may even reach 115%. Those results are very interesting because in real situation liquid droplets could come from an upstream condensation in the primary steam line or in the nozzle, and it might be tempting to think such condensation could have been harmful to the ejector operation. Those results tend to prove the contrary.

In order to understand this two-phase behavior, CFD simulations were performed with a simple discrete phase model for inert water droplets. The chosen condition were the cases $P_1^0 = 4bar$ and $P_b = 1.45bar$. Different tests have been performed with different droplet diameters and water mass fractions. Results are summarized on figure 12 for the $k - \epsilon$ and $k - \omega - sst$ models. For that condition, the experimental improvement in terms of entrainment ratio was about 12%. Numerical simulations were not able to predict such a behavior for any tested conditions. Indeed, for all tested conditions, numerical results

predict a decrease of the entrainment when droplets are injected into the primary stream. Those contradictory results were also mentioned in the thesis of Al-Ansary [14]. However, the quantitative differences presented in the current paper are less important and some interesting features can be highlighted owing to the larger number of numerical tests performed. Indeed, for a mass fraction of about 12% and a droplet diameter of $17\mu m$, which is the same order of magnitude of Al-Ansary et al. [16], the numerical decrease of the entrainment ratio is about 26% for the $k-\epsilon$ model and only 8% for the $k-\omega-sst$ model, while they noted 32% in their study. But comparative conclusions are difficult since Al-Ansary [14] does not provide any details on the modeling aspect, such as the drag model, boundary conditions (constant mass fraction of water for the different droplet size?), etc. Moreover, in the conditions matching the current experimental data ($\alpha_l = 1\% - 1.3\%$ and a droplet diameter of about $50\mu m$) the difference are even smaller. In addition, figure 12 shows that the harmfull effect for the entrainment rate is also larger if the water mass flow rate is high. Concerning the influence of droplet diameter, the results illustrate almost no effect for diameters larger than $15\mu m$, while the entrainment rate increases for higher diameters. This results is even more noticeable in the case of the $k-\omega-sst$ model where original entrainment rates without any droplet is reached back when droplet diameter is $5\mu m$. These CFD results raise the question about the hypothesis of Al-Ansary et al. [16] about a possible decrease of momentum irreversibilities providing higher entrainment rates when fine droplets are injected into the primary nozzle. However, other physical phenomena, which are not taken into account in this simple model, could be also involved in that observed behavior. Those phenomena could be droplet deposition into a film, annular water spray from nozzle lips and spray breakup coming from the film arrachement, etc: flow visualization could be performed

to investigate and assess such effects, allowing to set up improved model . The fraction of water in air could also modify the local thermodynamic properties such as the sound speed. This effect, which should be even more predominant in a condensing flows, will have to be investigated for refrigeration applications though advanced two-phase models being able to predict droplet nucleation, growing and none-equilibrium effects. But there is currently a serious lack in terms of ejector modeling and understanding in the case of two-phase flow with real fluids (effect of the inlet quality of primary and secondary flows, level of saturation or superheating, etc...).

Concluding remarks

In this paper an integrated and a balanced CFD-experiment study was presented for a supersonic ejector working with air. Using air to test and validate thermofluid models may be useful because experimental set is very simple and a wide range of measurement may be achieved compared to a closed refrigerant system. In this work, good validation results have been obtained for a wide range of operating conditions and were generally in a better quantitative agreement that those found in literature, especially for the off-design operation. It is believed such good results may be mostly attributed to the special focus of setting up a test bench with geometric and boundary conditions measurement as close as possible of those of the CFD. Those results allow to state that turbulence modeling is not a fully answered question for ejector operation and flow physics predictions. Indeed, even though the $k-\epsilon$ provided best results especially for the on-design-conditions, the $k-\omega-sst$ or other models should be considered and more studied for off-design predictions.

Furthermore, it has been highlighted that for exactly the same entrainment rate prediction over a large range of conditions, both models could provide very different local flow structures. This issue has to be addressed and will be the focused of the second part of this paper. This point is very critical because it clearly demonstrates that the link between a good validation in terms of a global ejector performance such as the entrainment rate and a good prediction of the local flow physics prediction is not guaranteed.

In addition, it has been clearly demonstrated that the presence of liquid droplets in the primary stream, which could physically come from condensation, is not necessarily harmful to the ejector operation but on contrary may improve its off-design operation. However, the argument of previous authors claiming that the presence of liquid droplets in the primary jet could reduce momentum irreversibility between both streams, and then enhance the entrainment rate, was not validated by a simple discrete phase model. The correct modeling of this observed behavior is then still an open question. Moreover, for a real refrigeration situation, a consistent compressible two-phase CFD model needs to be set up. In this sense, a good model for ejectors operating with refrigerants should take into account possible nucleation, growing of condensation droplets, metastable states, and should be consistent in terms of the mixture speed of sound. To our knowledge, there is no such works published in the open literature.

Acknowledgement

Author wish to acknowledge the General Directorate for Technology, Research and Energy (D.G.T.R.E.) of the Ministry for Belgium's Walloon Region to

financially support the PROFESSI project. Authors would also to thank all the technical staff of the TERM division for its help in the set-up of the experimental stand, and the company POLYSPRAY (info@polyspray.be) for providing and adjusting the ultra-sonic atomizer.

References

[1] K. Matsuo, Y. Miyazato, H. D. Kim, Shock train and pseudo-shock phenomena in internal gas flows, Progress in Aerospace Sciences 35 (1999) 33–100.

[2] Y. Bartosiewicz, Z. Aidoun, P. Desevaux, Y. Mercadier, Numerical and experimental investigations on supersonic ejectors, International Journal of Heat and Fluid Flow 26 (2005) 56–70.

[3] Y. Bartosiewicz, Z. Aidoun, Y. Mercadier, Numerical assessment of ejector operation for refrigeration applications based on cfd, Applied Thermal Engineering 26 (5-6) (2006) 604–612.

[4] S. B. Riffat, G. Gan, S. Smith, Computational fluid dynamics applied to ejector heat pumps, Applied Thermal Engineering 16 (4) (1996) 291–297.

[5] S. B. Riffat, P. Everitt, Experimental and cfd modelling of an ejector system for vehicle air conditioning, Journal of the Institute of Energy 72 (1999) 41–47.

[6] B. J. Huang, V. A. Petrenko, J. M. Chang, C. P. Lin, S. S. Hu, A combined cycle refrigeration system using ejector-cooling as the bottom cycle, International Journal of Refrigeration 24 (5) (2001) 391–399.

[7] K. Chunnanond, S. Aphornratana, Ejectors: Applications in refrigeration technology, Renewable & Sustainable Energy Reviews 8 (2004) 129–155.

[8] D. W. Sun, I. W. Eames, Recent development in the design theories and applications of ejectors - a review, Journal of the Institute of Energy 68 (1995) 65–79.

[9] S. B. Riffat, L. Jiangang, G. Gan, Recent development in ejector technology - a review, International Journal of Ambient Energy 26 (1) (2005) 13–26.

[10] E. Rusly, L. Aye, W. W. S. Charters, A. Ooi, Cfd analysis of ejector in a combined ejector cooling system, International Journal of Refrigeration 28 (2005) 1092–1101.

[11] T. Sriveerakul, S. Aphornratana, K. Chunnanond, Performance prediction of steam ejector using computational fluid dynamics: Part 1. validation of the cfd results, International Journal of Thermal Sciences 46 (8) (2007) 812–822.

[12] T. Sriveerakul, S. Aphornratana, K. Chunnanond, Performance prediction of steam ejector using computational fluid dynamics: Part 2. flow structure of a steam ejector influenced by operating pressures and geometries, International Journal of Thermal Sciences 46 (8) (2007) 823–833.

[13] Y. Bartosiewicz, Z. Aidoun, P. Desevaux, Y. Mercadier, Cfd-experiments integration in the evaluation of six turbulence models for supersonic ejector modeling, in: Integrating CFD and Experiments Conference, Glasgow,UK, 2003.

[14] H. A. M. Al-Ansary, Study of single-phase and two-phase ejectors, Ph.D. thesis, Georgia Institute of Technology (2004).

[15] K. Pianthong, W. Seehanam, M. Behnia, T. Sriveerakul, S. Aphornratana, Investigation and improvement of ejector refrigeration system using computational fluid dynamics technique, Energy Conversion and Management, in press.

[16] H. A. M. Al-Ansary, S. M. Jeter, Numerical and experimental analysis of single-phase and two-phase flow in ejectors, HVAC & R Research 10 (4) (2004) 521–538.

[17] S. A. Morsi, A. J. Alexander, An investigation of particle trajectories in two-phase flow systems, Journal of Fluid Mechanics 55 (2) (1972) 193–208.

[18] M. Wolfstein, The velocity and temperature distribution of one-dimensional flow with turbulence augmentation and pressure gradient, International Journal of Heat and Mass transfer 12 (1969) 301–318.

[19] ESDU, Ejectors and et pumps, data item: 92042 (1992).

[20] ASHRAE Guide and Data Book Equipment, Chapter 13, Steam-Jet refrigeration Equipment (1969).

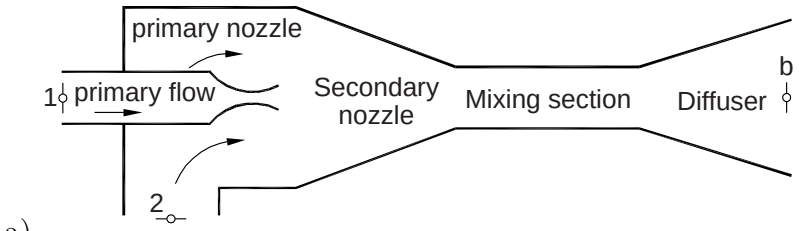

a)

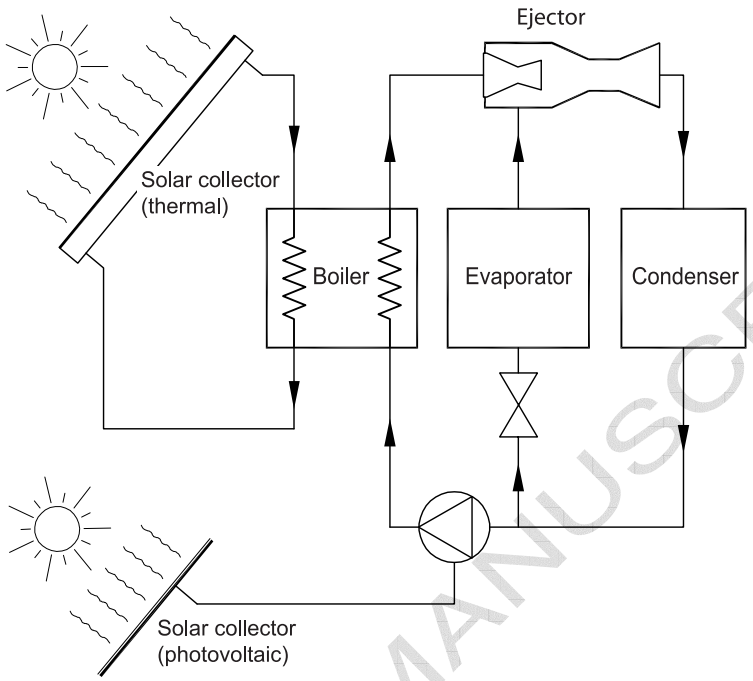

b)

Figure 1. A typical ejector geometry (a). A supersonic ejector in a solar air-conditioning cycle (b)

a)

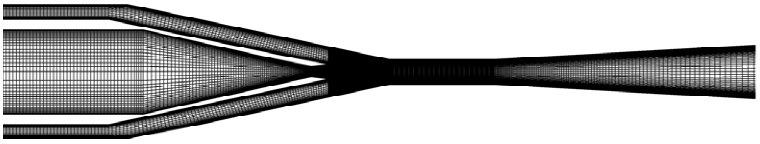

b)

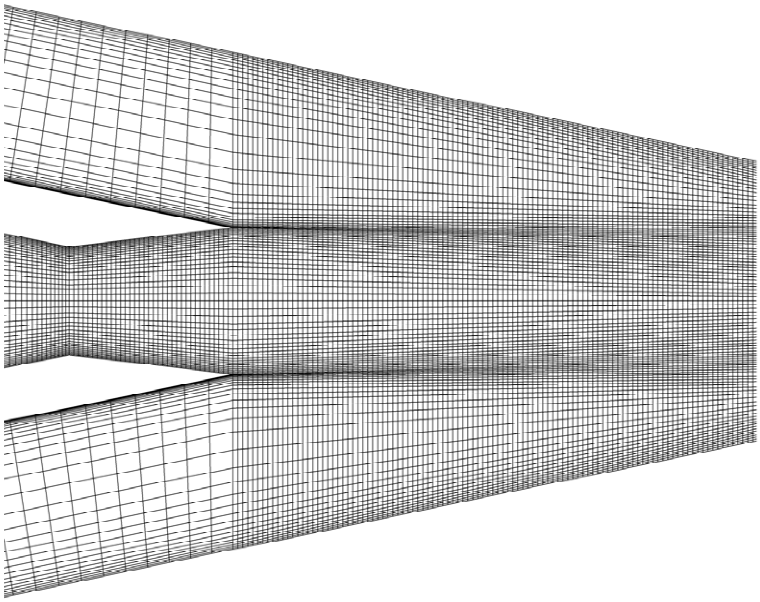

Figure 2. Computational mesh

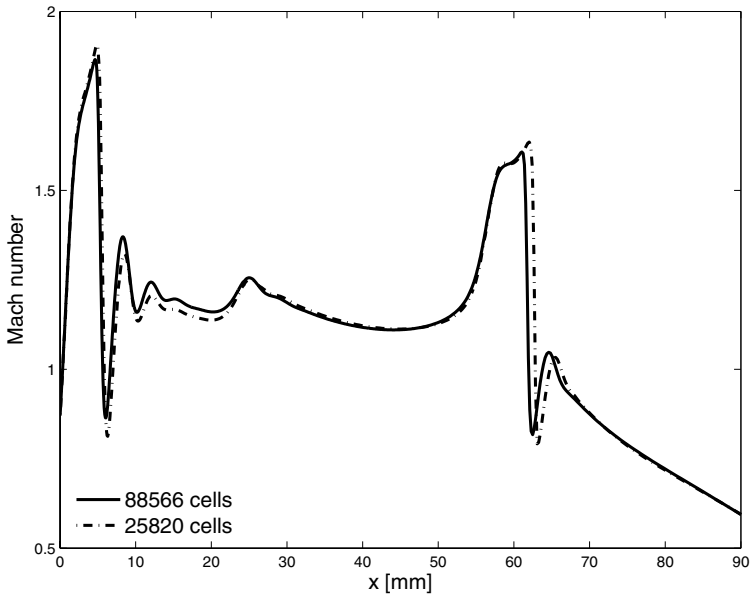

Figure 3. Mesh convergence: centerline Mach number

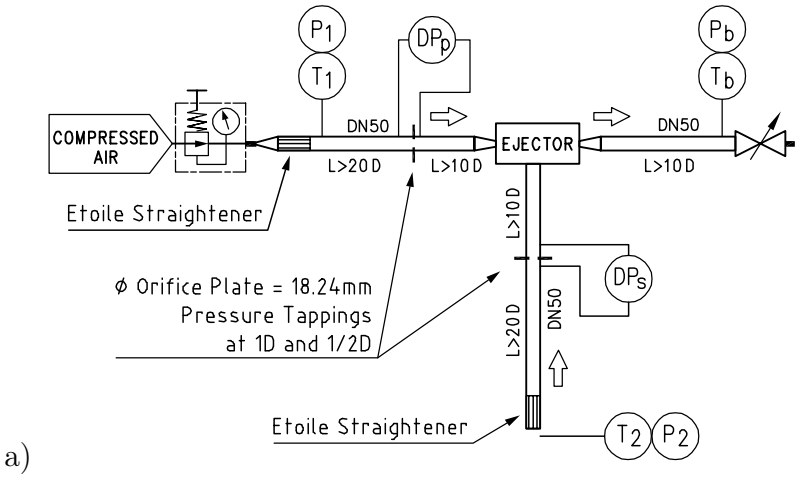

a)

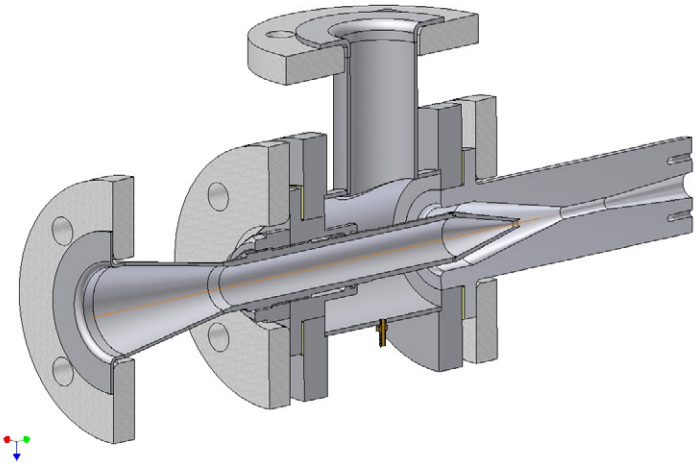

b)

Figure 4. Sketch of the experimental set-up (a). A 3D view of the ejector geometry (b)

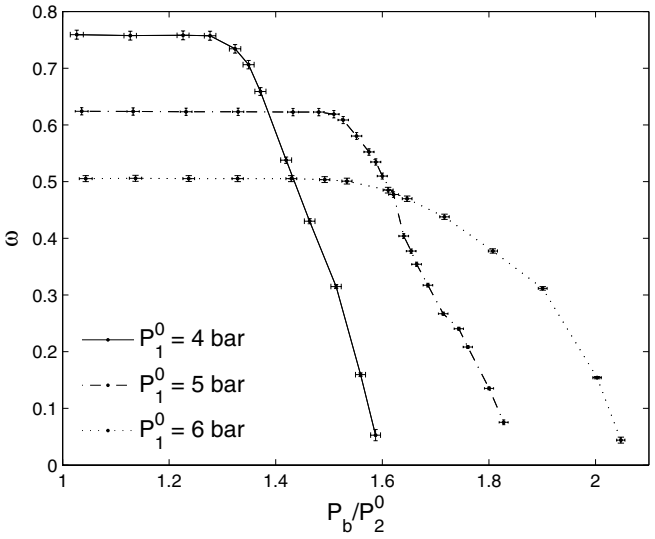

Figure 5. Ejector characteristics- Experimental results

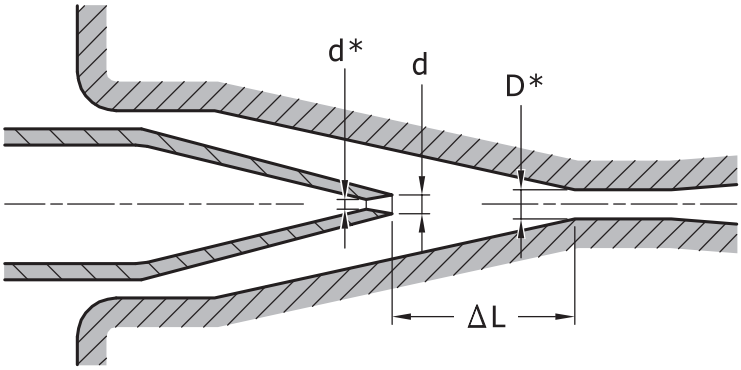

Figure 6. Main ejector dimensions

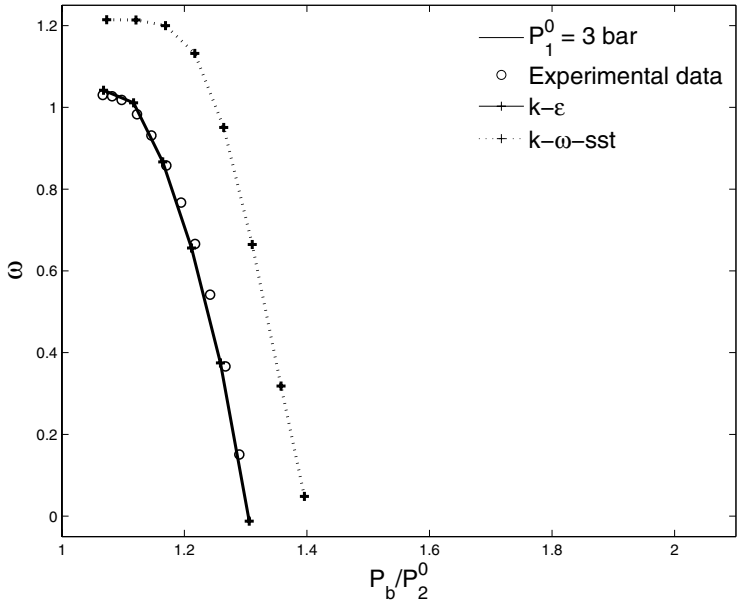

a)

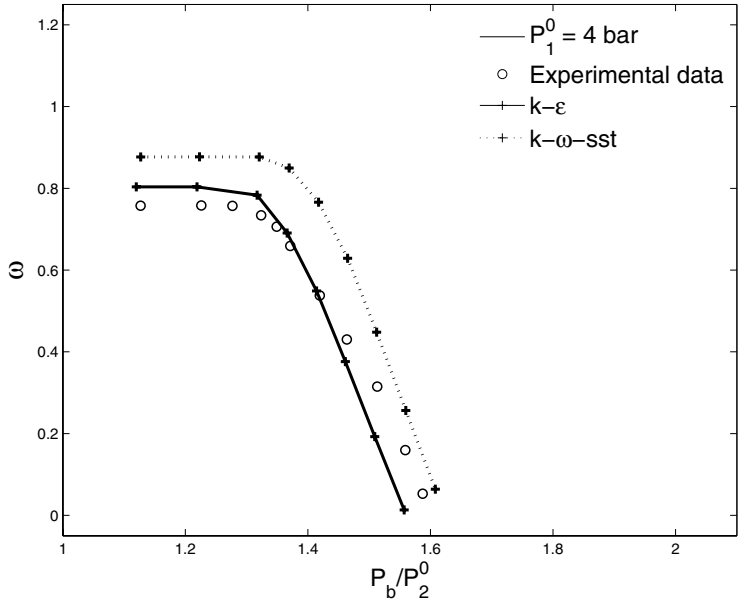

b)

Figure 7. Comparison CFD-experiments for $P_1^0 = 3bar$ (a) and $P_1^0 = 4bar$ (b)

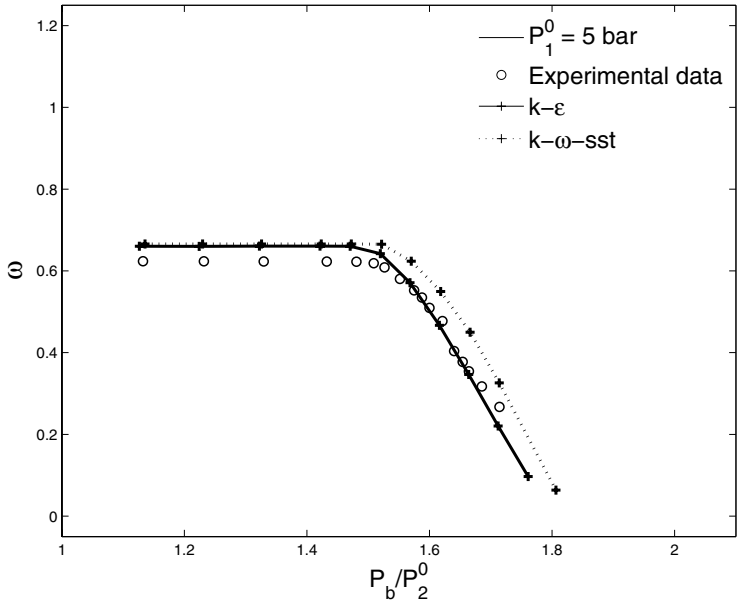

a)

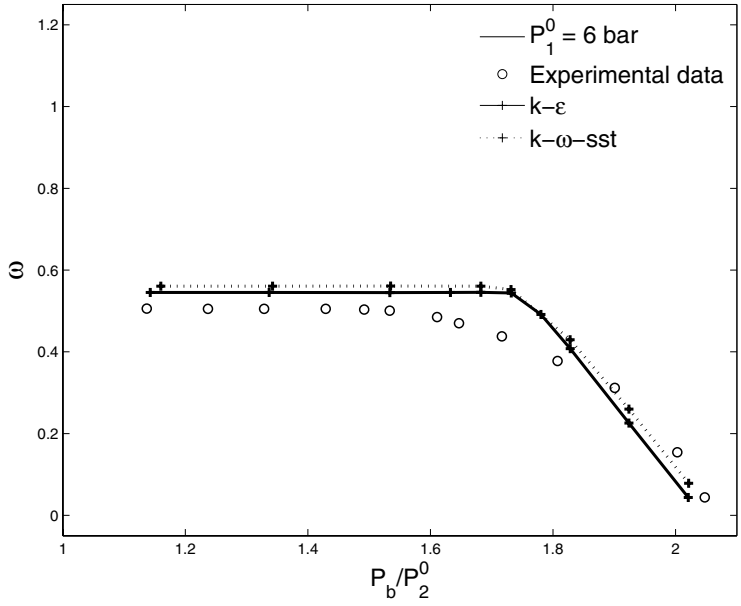

b)

Figure 8. Comparison CFD-experiments for $P_1^0 = 5bar$ (a) and $P_1^0 = 6bar$ (b)

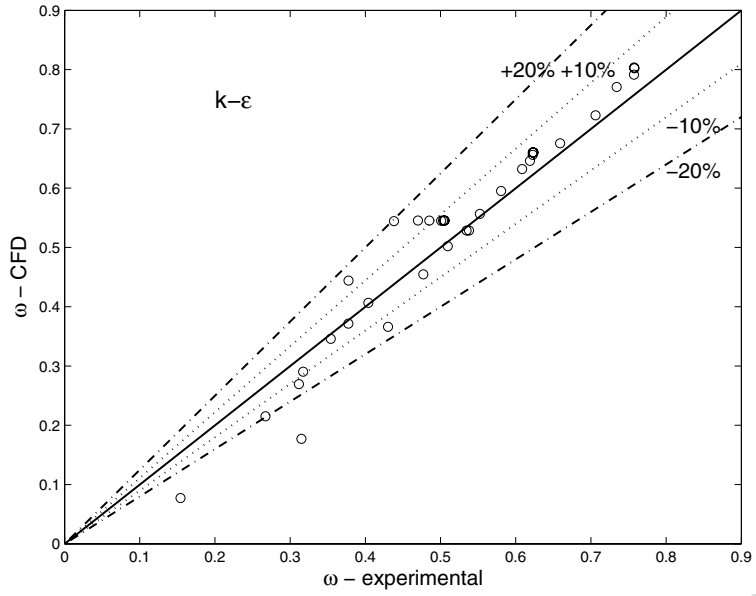

a)

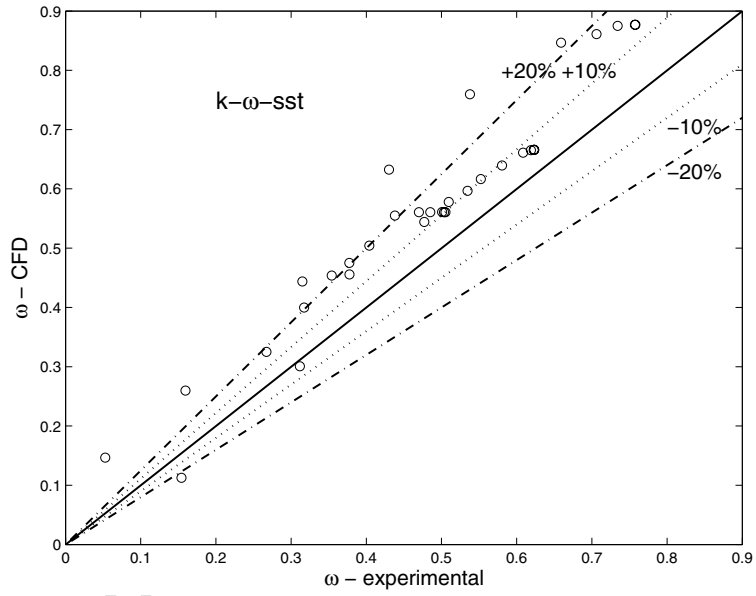

b)

Figure 9. Errors distribution for $k-\epsilon$ (a), $k-\omega-sst$ (b)

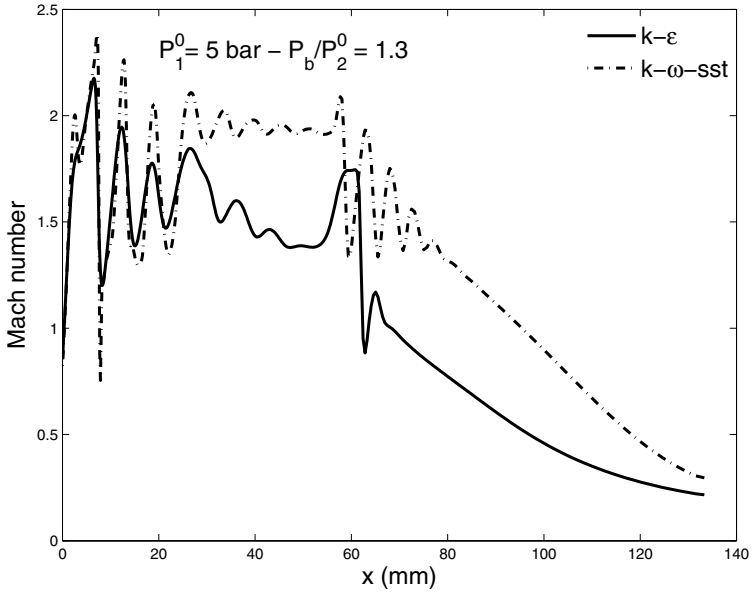

Figure 10. Centerline Mach number for $P_1^0 = 5bar$ and $P_b/P_2^0 = 1.3$

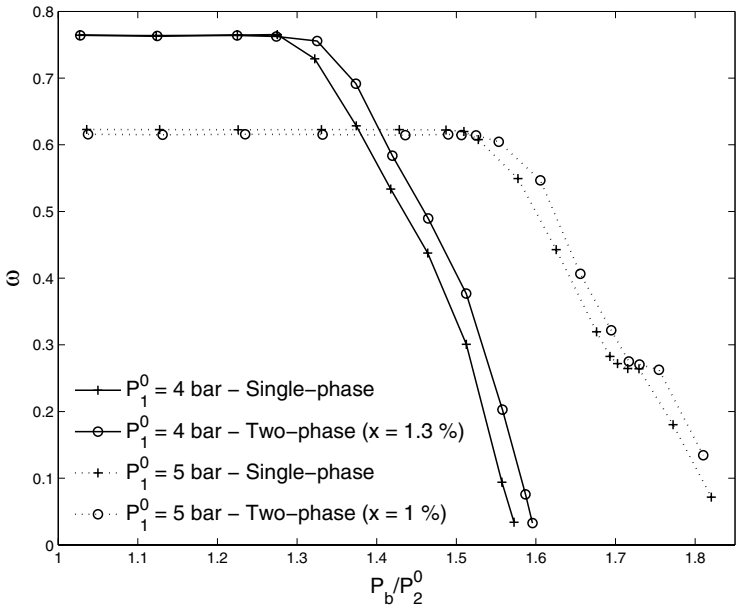

Figure 11. Entrainment ratio: single-phase vs. two-phase flow

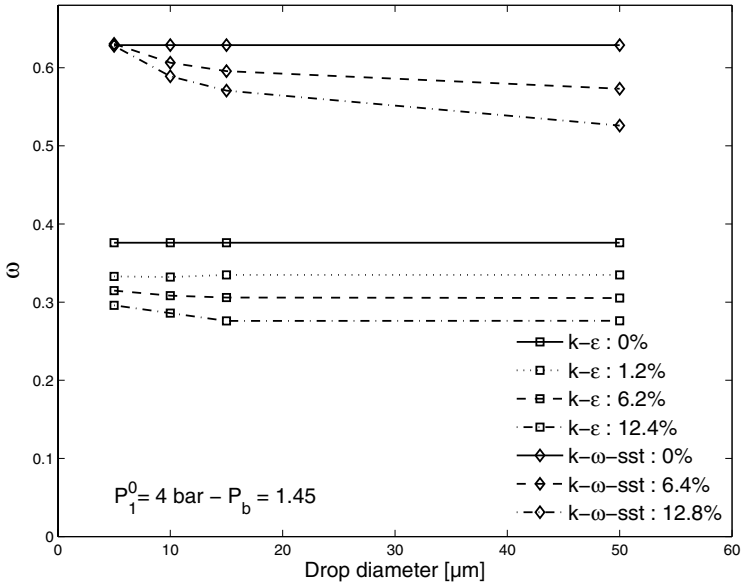

Figure 12. Entrainment ratio as a function of droplet diameter for different water mass fraction α_l

Nomenclature

d	$[m]$	Diameter
F_D	$[s^{-1}]$	Drag force coefficient
F_p	$[N]$	Drag force
$\dot{m}$	$[m.s^{-1}]$	Mass flow rate
P	$[bar]$	Pressure
x	$[mm]$	Axial location from the throat of the primary nozzle
α_l	$[-]$	Water mass fraction
μ	$[kg.m^{-1}.s^{-1}]$	viscosity
ω	$[-]$	Entrainment ratio
ρ	$[kg.m^{-3}]$	Density

Subscripts, superscripts:

0	Total, stagnation property
1	Primary flow inlet
2	Secondary flow inlet
b	property at back (ejector outlet)
l	Laminar
p	Particle
t	Turbulent